Available online at www.sciencedirect.com
ScienceDirect
Advances in Space Research 40 (2007) 794–801
ADVANCES IN SPACE RESEARCH (a COSPAR publication)
www.elsevier.com/locate/asr

The sensitivity of mesospheric ice layers to atmospheric background temperatures and water vapor

Franz-Josef Lübken *, Markus Rapp, Irina Strelnikova

Leibniz Institute of Atmosphere Physics, Schloss-Str. 6, 18225 Kühlungsborn, Germany

Received 18 July 2006; received in revised form 2 January 2007; accepted 4 January 2007

Abstract

Several thousand runs of a microphysical ice particle model have been performed to investigate the sensitivity of ice layers on background temperatures and water vapor in the summer polar mesopause region. Non-linear processes lead to unexpected variations of volume backscatter coefficients (BSC) as observed by lidars, and polar mesosphere summer echoes (PMSE) as observed by radars. Generally speaking, decreasing temperatures and increasing water vapor leads to larger BSC. However, very low mesopause temperatures can lead to a decrease of BSC because many small ice particles are generated which are more difficult to observe compared to fewer and bigger particles. Varying the temperature profile around a climatological mean we find that the temperature at the altitude of maximum BSC decreases with a slope of approximately −1.9 K/km which is significantly less negative than the atmospheric temperature gradient at typical NLC altitudes (−6.1 K/km). Increasing the water vapor concentration (=[H_2O]) leads to an increase of BSC magnitude and to a decrease of the maximum BSC altitude which varies exponentially with [H_2O]. The corresponding scale height is $H_{BSC} \sim 1.36$ km. Some of these variations differ significantly from simple lapse rate considerations because of non-linear effects involved. Our model results have important implications for the comparison of ice layer characteristics in the southern and northern hemisphere. Furthermore, they allow to verify long term variations of temperatures and water vapor variations predicted by GCM models.

Keywords: Summer polar mesosphere; Ice layers; Noctilucent clouds; Polar mesosphere summer echoes; Summer mesopause; High latitudes; Ice clouds

1. Introduction

Ice layers in the summer mesopause region are known as 'noctilucent clouds' (NLC) if observed from the ground (by naked eye or by lidars) or as 'polar mesospheric clouds' (PMC) if observed from satellites. Several remote sensing and insitu measurements have shown that they mainly consist of water ice and are therefore closely related to the very low summer mesopause temperatures at middle and polar latitudes (e.g., Gadsden and Schröder, 1989; Lübken et al., 1996; Hervig et al., 2001; Fiedler et al., 2003; Höffner et al., 2003). More precisely, ice particles are generated and increase in size if the degree of saturation (S) is large enough. As has been fully explained only recently, very strong radar echos known as '(polar) mesosphere summer echoes', (P)MSE, are closely linked to charged ice particles and therefore also require very low temperatures and a sufficiently large amount of water vapor (see review by Rapp and Lübken, 2004). The existence and morphology of these ice layers are often used to infer information about the background atmosphere, in particular on temperatures and water vapor in the mesosphere/lower thermosphere region (MLT). For example, the small difference of NLC parameters observed by lidar in the northern and southern hemisphere, respectively, has led to conclusions about potential hemispheric differences in the thermal structure of the upper atmosphere (Chu et al., 2006). Similar differences in satellite observations of PMC have stimulated model simulations to explain inter-hemispheric variations (Bailey et al., 2005; Siskind et al., 2005; Hervig and Siskind, 2006).

A better understanding of the influence of background parameters on ice layers is also required to evaluate model

* Corresponding author. Tel.: +49 38293 680; fax: +49 38293 6850.
E-mail address: luebken@iap-kborn.de (F.-J. Lübken).

0273-1177/$30
doi:10.1016/j.asr.2007.01.014

predictions on long term and/or solar cycle variations of temperatures and water vapor in the MLT region (Khosravi et al., 2002; Schmidt et al., 2006). The trends derived in these models can be transferred to expected changes in ice layers which can be evaluated by observations. We have performed nearly 10,000 model runs with the microphysical model CARMA (Community Aerosol and Radiation Model for Atmospheres) varying the background profiles of temperatures and water vapor. The CARMA model is described in the next section and the results are presented and discussed in Sections 3 and 4.

2. The CARMA model

2.1. The community aerosol and radiation model for atmospheres: CARMA

CARMA is a flexible three-dimensional microphysical model developed over the past 25 years, and has been applied to a wide variety of problems ranging from cloud physics to aerosols on Earth and on other planets. The model originates from a one-dimensional stratospheric aerosol code developed by Turco et al. (1979) and Toon et al. (1979). CARMA was first applied to the physics of mesospheric ice particles by Turco et al. (1982), and then further developed by Jensen et al. (1989), and Jensen and Thomas (1994), the latter being a two-dimensional study of the effect of gravity waves on the formation of NLC/PMC. This work was then extended by Rapp et al. (2002) who treated gravity wave/NLC interactions for wave parameters which were determined from rocket borne in situ observations of winds and temperatures during simultaneous and nearly common volume measurements of NLCs by lidar.

For the current study, we use a one-dimensional version of CARMA which has recently been described in detail in Rapp and Thomas (2006). In short, the current model domain comprises 120 altitude levels from 72 to 102 km altitude, and the ice and meteor smoke particle size distributions are evaluated on radius grids consisting of 40 non-equally spaced size bins between 2 and 900 nm for ice particles, and 0.25–112.6 nm in the case of meteor smoke particles, which act as ice nuclei. Transport of aerosol particles and water vapor by the mean vertical wind and eddy diffusion is handled by an Eulerian transport scheme.

As our reference background atmosphere we have adopted the temperature and neutral number density profile from Lübken (1999) for a latitude of 69°N and July, 1. The vertical wind profile for the same latitude and time has been taken from the study by Berger and von Zahn (2002), and the eddy diffusion profile has been adapted from the collection of turbulence measurements at 69°N under polar summer conditions published by Lübken (1997). The basic-state water vapor mixing ratio has been taken from the model simulations by Körner and Sonnemann (2001). Finally, water vapor equilibrium pressures given by Murphy and Koop (2005) have been used.

In Fig. 1 we show the temporal development of ice particle number densities, NLC, and PMSE, respectively, for a typical polar summer MLT temperature profile with a mesopause temperature of 130 K located at 88 km and a temperature of 150 K at 82 km. The NLC signal in this Figure is given as the ratio of the backscatter signal from ice particles to the background molecular signal at the same altitude ('backscatter ratio'). The PMSE signal is given in terms of a proxy $P = N_A \cdot Z_A \cdot r_A^2$ introduced by Rapp et al. (2003). N_A, Z_A, and r_A are the number density, charge, and radius of ice particles. It should be noted that some physical processes required to produce PMSE are not included in this proxy, for example turbulence. As can be seen from Fig. 1 an ice layer develops and reaches quasi-stationary conditions after several hours. We use the ice cloud parameters at 24 h after initialization. The NLC covers only the lower part of the ice layer, whereas PMSE extends to higher altitudes and covers nearly the entire altitude range filled with ice particles. This feature is mainly explained by the fact that NLC and PMSE have different sensitivity to ice particle radii, namely $\sim r^6$ and $\sim r^2$, respectively. Roughly speaking the lidars (NLC) see only the largest ice particles (approximately >20 nm), whereas radars (PMSE) are less sensitive to radius and cover basically the entire population. The CARMA results shown in Fig. 1 are nicely confirmed by many observations of NLC and PMSE (e.g., Nussbaumer et al., 1996; Lübken et al., 2004b). It is interesting to note that the ice cloud extends to altitudes above and below the $S = 1$ line. This is caused such as transport processes such as sedimentation and turbulent diffusion.

3. Results from CARMA

We have systematically varied the temperature and water vapor profiles starting with default profiles (see above) which reflect our current knowledge of the mean

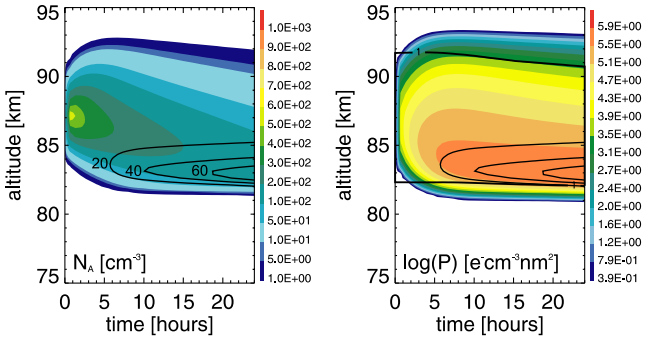

Fig. 1. CARMA model results of the temporal development of ice particle number densities (left), PMSE proxy (log scale, right), and NLC signal (backscatter ratio, thin black lines in left and right panels). The thick black line in the right panel represents $S = 1$. The definitions of the PMSE proxy and the backscatter ratio are given in the text. A standard background temperature profile with a mesopause temperature of 130 K located at 88 km and a temperature of 150 K at 82 km has been used in the CARMA model run.

state at high latitudes. In total we have performed several thousand CARMA model runs combining various background profiles.

3.1. Sensitivity to background temperatures

In Fig. 2 we show two slightly different temperature profiles which are based on climatologies for high latitude stations in the northern and southern hemisphere, namely Andøya (70°N, July), and Rothera (68°S, late January) (Lübken, 1999; Lübken et al., 2004a). At NLC/PMSE altitudes the temperature profiles differ very little, for example by only 4 and 7 K at 82 and 88 km, respectively. Using these temperature profiles we have used CARMA to determine the corresponding PMSE and NLC profiles. As can be seen from Fig. 3 a slight increase in temperatures around the mesopause leads to a large decrease in NLC backscatter ratio (from 14 to 5) and to an increase in mean altitude by more than a kilometer. The PMSE proxy decreases by almost an order of magnitude (10 dB) but the mean PMSE altitude remains nearly unchanged.

We have systematically varied the temperature profile around the mesopause and studied its effect on NLC and PMSE. In Fig. 4 we show backscatter coefficients (BSC) for temperature profiles with a fixed mesopause altitude (88 km), a mesopause temperature (T_M) varying from 120 to 140 K, and a fixed temperature of 150 K at 82 km. Between these fix points the temperature profiles were interpolated and extended in a self-evident way taking into account typical temperature gradients in the MLT region. We use the backscatter coefficient at $\lambda = 532$ nm as a measure of NLC since it is frequently derived from lidar measurements (see, for example, Fiedler et al., 2003 which also contains a detailed description of BSC). As can be seen from Fig. 4 the BSC signal does not increase steadily with

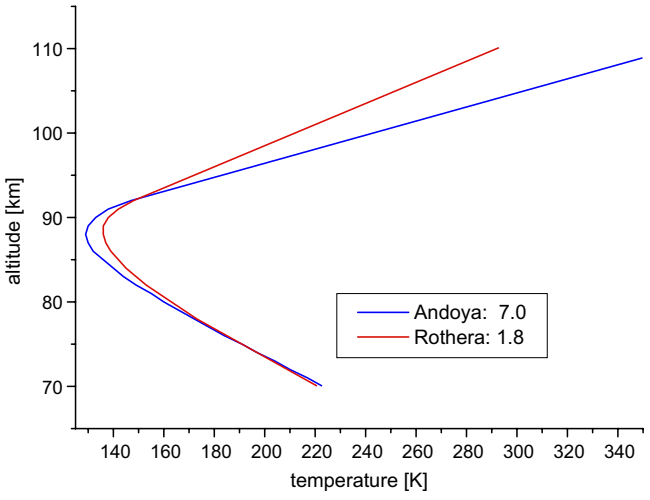

Fig. 2. Temperature profiles based on climatologies for high latitude stations in the northern and southern hemisphere. Blue: Andøya (70°N, July). Red: Rothera (68°S, late January). (For interpretation of the references to colour in this figure legend, the reader is referred to the web version of this article.)

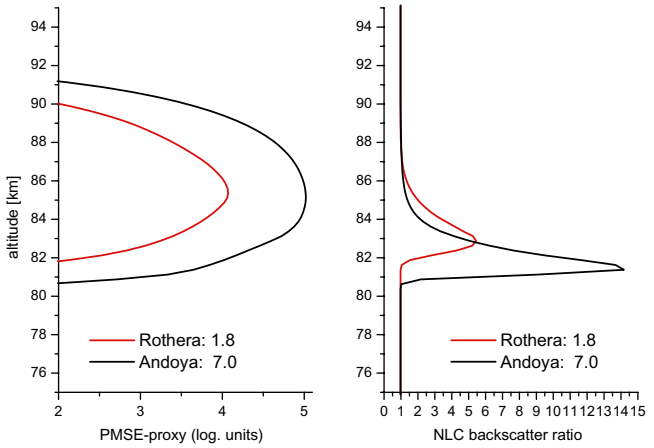

Fig. 3. PMSE proxy (left) and NLC backscatter ratio (right) calculated with CARMA using the temperature profiles from Fig. 2.

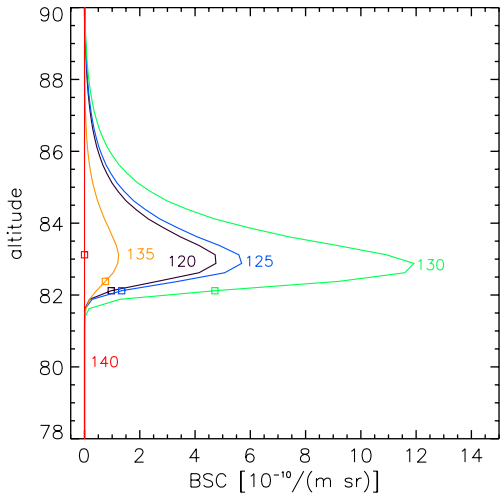

Fig. 4. Backscatter coefficients for temperature profiles with mesopause temperatures from 120 to 140 K, given in the plot. The mesopause altitude (88 km) and the temperature at 82 km are fixed (150 K). The squares mark the altitudes where $S = 1$.

decreasing temperature but instead shows a maximum around $T_M = 130$ K. A detailed analysis of CARMA results shows that the decrease of BSC with decreasing temperature (below appr. 130 K) is caused by the fact that many small particles are generated at very low temperatures. A temperature increase leads to fewer but larger particles which cause stronger BSCs. Indeed, simultaneous observations of temperatures and NLC have shown that NLC are weak or absent if the mesopause temperature is extremely low (see Fig. 9 in Lübken et al., 1996). We note that for a mesopause temperature of 140 K no ice particles are created. The PMSE layer parameters show a more regular variation with mesopause temperatures (not shown here). In Fig. 4 we also show the altitude where $S = 1$, which is significantly below the maximum BSC. This is surprising since particles should grow and lead to larger BSC as long as S is larger than unity. We have studied the CARMA output in detail and identified several mechanisms

which can explain this effect. The number density of particles rapidly decreases below ~84 km thereby decreasing the BSC. Furthermore, the degree of saturation used in Fig. 4 is somewhat too large because the following effects were not considered: (i) the particle temperature is slightly larger (by less than 1 K) compared to atmospheric temperatures and (ii) the Kelvin effect leads to a slightly larger saturation pressure (by ~10%) for particles with radii of approximately 40 nm (compared to $r_A = \infty$) (see for more details Berger and von Zahn, 2002; Rapp and Thomas, 2006).

Another set of CARMA model runs was performed where we shifted the entire temperature profile (not only the mesopause temperature as for Fig. 4) by ±5 and ±10 K starting with our standard profile given by a mesopause at 88 km/130 K and a fixed temperature of 150 K at 82 km. As can be seen in Fig. 5 the peak altitudes of NLC and PMSE increase linearly with temperature shift with a rate of 0.24 km/K. The altitudes of maximum NLC and PMSE are therefore more sensitive to temperature changes than expected from the mean atmospheric lapse rate (−6.1 K/km) which implies a sensitivity of only 0.16 km/K. The reason for the difference is the freeze drying effect which accumulates increasingly more water vapor at the bottom of the profile with decreasing temperatures (this point will be further elucidated in the next section). Regarding PMSE, the altitudes of the proxy maximum coincide exactly with the altitudes of maximum BSC. As discussed already in Fig. 4 the altitude of $S = 1$ is somewhat below the altitude of maximum BSC.

In the right panel of Fig. 5 the corresponding magnitudes of NLC and PMSE are shown. As noted earlier the NLC signal drastically depends on temperatures, whereas the PMSE magnitude is much less sensitive. The main reason for this behavior is the different sensitivity on the particle size which is given by the total amount of water vapor available for ice particle formation. The large sensitivity of NLC and PMSE altitudes to temperature changes (even larger than expected from the background lapse rate) demonstrates the importance of non-linear processes on ice layer parameters. We note that the magnitudes of BSC and PMSE increase steadily with decreasing temperatures, which is somewhat different than noted in Fig. 4. The reason for this is that the temperature profiles used in Fig. 5 are shifted at all altitudes, i.e., they cover an increasingly large altitude range with supersaturation when temperature decreases. By contrast the temperatures used for Fig. 4 were varied around the mesopause only.

Finally, we show a collection of 144 temperature profiles in Fig. 6 being used in CARMA to determine NLC and PMSE characteristics. Some of the temperature profiles are presumably at the limit of what is actually observed in the real atmosphere. As an example of the results deduced from these studies we show the altitude of maximum BSC as a function of temperature at that altitude in Fig. 7. Different from the results shown in Fig. 5 where the temperature profiles where simply shifted relative to a standard profile, various mesopause temperatures and temperature gradients at NLC altitudes have been used to determine these BSCs (see Fig. 6). In general, temperatures at the altitude of maximum backscatter are lower if the layers appear at higher altitudes. We have fitted a straight line fit to the points given in Fig. 7 and find a slope of −1.9 K/km. In other words a temperature change of only 1.9 K is required to change the BSC peak by 1 km. This is significantly less than expected from the mean atmospheric lapse rate of −6.1 K/km. We will discuss the implications of this result in Section 4.

3.2. Sensitivity to water vapor

We have also varied the water vapor profiles to study their effect on the mean characteristics of NLC and PMSE.

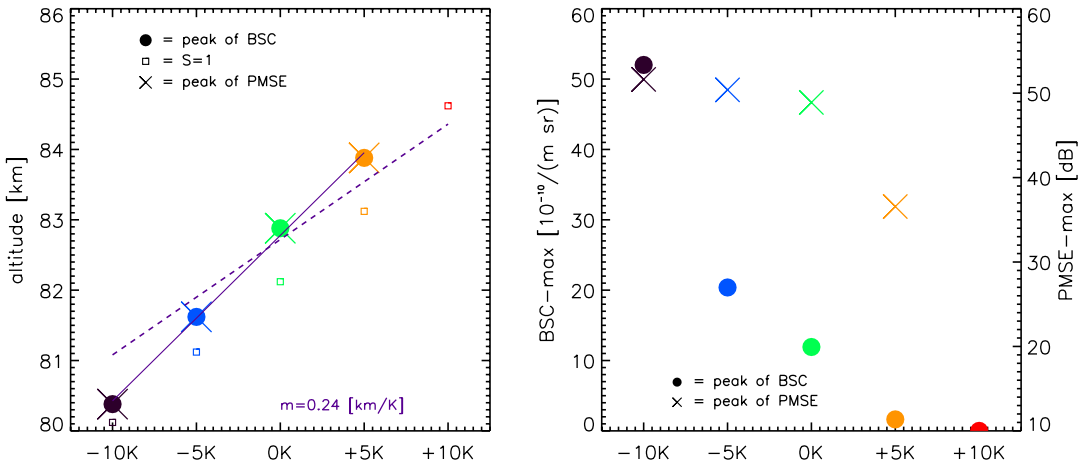

Fig. 5. Left: altitude of maximum BSC (bullets) and PMSE (crosses) for temperature profiles shifted by −10, −5, 0, +5, and +10 K relative to a default reference profile (see text). A straight line fit to the maximum BSC values yields a slope of 0.24 km/K (solid line). For comparison the line corresponding to the mean atmospheric lapse rate 0.16 km/K is also shown (dotted line). Right: corresponding magnitudes of the maximum BSC and PMSE signals. For the +10 K profile no NLC and PMSE developed.

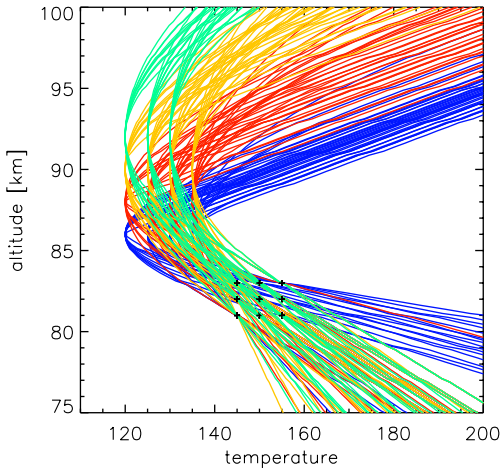

Fig. 6. A selection of 144 temperature profiles used in CARMA to study the variation of ice layer parameters with background temperature.

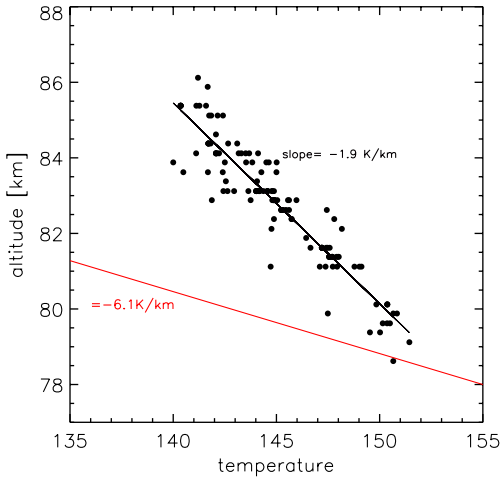

Fig. 7. The altitude of maximum BSC (dots) as a function of temperature at that altitude. The temperature profiles shown in Fig. 6 were used. The red line indicates a typical atmospheric temperature gradient at NLC altitudes of −6.1 K/km. (For interpretation of the references to colour in this figure legend, the reader is referred to the web version of this article.)

The 'standard' profile (see above) has been multiplied by factors varying from 0.3 to 10. In Fig. 8 we show frost point temperatures (T_{frost}) and BSC profiles resulting from these modified H_2O profiles, whereas the atmospheric temperature profile is kept unchanged, namely to our standard case. Increasing the water vapor concentration leads to a large increase in BSC signal and a decrease of the altitude where the maximum appears. As discussed already in Fig. 4 the altitude of $S = 1$ is again somewhat below the altitude of maximum BSC. As can be seen from Fig. 8 (left panel) the altitude where $S = 1$ decreases with increasing water vapor. This decrease is enhanced by a local accumulation of water vapour at the bottom of the $S = 1$ height range which leads to a local enhancement of T_{frost}. The magnitude of this local enhancement increases with total water vapor concentration and finally leads to a non-linear variation of maximum BSC altitude and magnitude. As can be seen from Fig. 9 (left panel) the altitude of maximum BSC decreases exponentially with increasing amount of water vapor. From a fit we derive a 'scale height' for the BSC peak altitude change of 1.36 km. This implies, for example, that a factor of 2 increase in water vapor decreases the altitude of maximum BSC by $|\log_e(1/2) \cdot 1.36| = 0.94$ km. The sensitivity of the maximum BSC signal on H_2O is shown in Fig. 9 (right panel). As expected the BSC maximum increases with the amount of water vapor available for particle formation (=[H_2O]). Ignoring very large and very small changes, the maximum signal increases with $[H_2O]^{2.3}$ which is close to the sensitivity expected from the very simple assumption that the BSC varies with r_A^6, therefore, with the square of the volume and mass, namely $\sim[H_2O]^2$. In reality ice particle growth leads to an entire spectrum of particles and several non-linear processes sensitive to H_2O and r_A are involved.

As mentioned above we have multiplied the default water vapor profiles by several factors, independent of altitude. In general we expect that the BSC change depends on the altitude profile of the water vapor change. We argue,

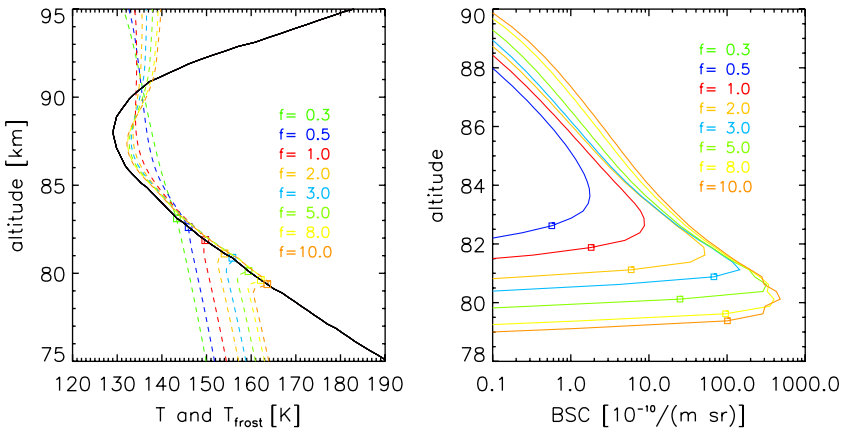

Fig. 8. Altitude profiles of frost point temperatures (left panel) and BSC (right panel) for water vapor profiles differing from the 'standard' profile (see text) by a factor (f) given in the inlet. The black line (left panel) represents the atmospheric temperature profile. The small squares mark the altitude where $S = 1$.

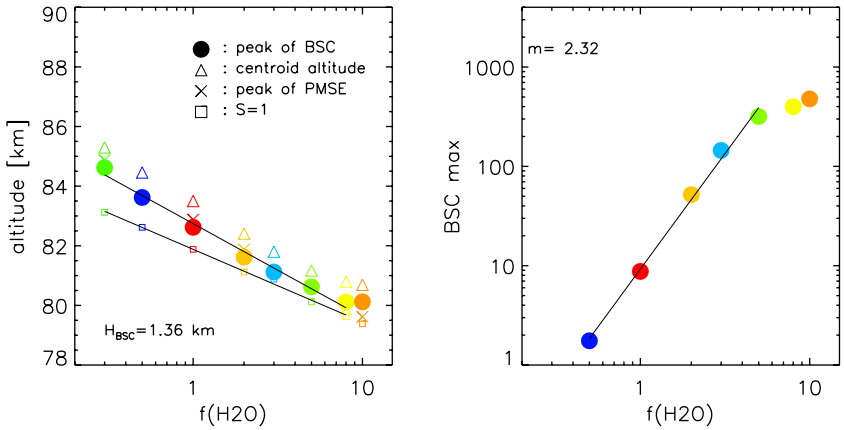

Fig. 9. Left panel: altitudes of maximum BSC (bullets) as a function of the factor f(H2O) used to modify the standard H_2O profile. Same for NLC centroid altitude (triangles), PMSE (crosses), and $S = 1$ (squares). The straight line fit (black line) corresponds to a 'scale height' of 1.36 km. Right panel: variation of the maximum BSC signal as a function of f(H2O). The maximum BSC varies exponetially as $\sim f^{2.32}$ (black line).

however, that this effect is of secondary importance since the main effect is caused by the total amount of water vapor available for particle growth, regardless at which altitude it is supplied.

We have also studied the effect of water vapor changes on PMSE and find similar effects seen in NLC but significantly smaller in magnitude (not shown here).

4. Discussion and conclusions

We have performed several thousand CARMA model runs varying the background temperature and water vapor profile. We realize that other atmospheric parameters such as vertical winds, meteoric influx, and eddy diffusivity will also affect the ice layer morphology. We also note that some atmospheric background parameters are interrelated, e.g., temperature and vertical winds. However, low enough temperatures and a significant amount of water vapor are presumably the most important ingredients to create ice particles in the MLT region. We have assumed stationary conditions in CARMA, i.e., no temporal variability. Certainly, the real atmosphere shows short and long term temperature variations caused by gravity waves, etc. As has been shown by Rapp et al. (2002) natural variability modifies the ice layer where the impact depends on the magnitude and time scale of the variations. It could be, however, that on a long term statistical basis these fluctuations do not significantly alter the mean characteristics of ice layers such as the mean altitude distribution of particle radii and number density. This study aims at improving our understanding of some basic microphysical processes involved in ice particle formation, whereas the entire temporal and spatial variability can only be covered by sophisticated 3d models (see, e.g., Berger and Lübken, 2006). However, the interpretation of the results from this type of models is complicated by the fact that many physical processes interact with each other, so that the influence of one particular process cannot easily be identified. The aim of the present study is exactly this, namely to study the influence of a particular process realizing that some other processes have been ignored.

Given a certain distribution of r_A and N_A the backscatter coefficient for a given wavelength (here: $\lambda = 532$ nm) can easily be calculated and compared to lidar observations of NLC. Regarding PMSE the situation is more complicated since various other ingredients are required to create PMSE, for example turbulence and sufficient ionization. This implies that PMSE may not be visible although temperatures are very low and ice particles are present. We therefore hesitate to discuss our PMSE results in detail but instead concentrate on NLC.

We now apply our results to NLC measurements recently published in the literature. Chu et al. (2006) reported NLC observations from a southern hemisphere (SH) station (Rothera, 68°S) and find a mean centroid altitude of 84.1 km. This is somewhat higher compared to a northern hemisphere (NH) co-latitude station (ALOMAR, 69°) where a mean centroid altitude of $z_c = 83.3$ km is observed (Fiedler et al., 2003). We will ignore in this study that (i) the lidars differ in wavelength, sensitivity, etc., (ii) that the statistics in the SH is poorer compared to the NH (128 versus 826 h of NLC), and (iii) that the BSC peaks show a natural short and long term variability of ~1 km at each station which covers a part of the height difference mentioned above. We will instead study the implications for the altitude difference if(!) it were solely due to temperature or water vapor change. As has been shown by our CARMA results presented above we cannot simply use the mean atmospheric temperature gradient at NLC altitudes to convert the NLC altitude difference to a temperature difference. Instead we have to take into account nonlinear effects. According to the results presented in Fig. 7 a height difference of 0.8 km corresponds to a temperature change of only 1.5 K which is certainly within the natural variability of the upper atmosphere and is too small to be detected by current instrumental capabilities. From our

studies in Section 3.2 we conclude that the same altitude difference can alternatively be explained by a 44% reduction of H_2O in the SH compared to the NH. Current water vapor measurements in the high latitude summer mesosphere are not accurate enough to exclude such an inter-hemispheric difference.

We conclude that the SH/NH difference of mean NLC altitudes corresponds to a temperature difference of 1.5 K or a H_2O difference of 44%, or a combination of both. We thereby ignore other potential reasons of either instrumental or geophysical origin. We note that PMSE have recently been observed in the southern hemisphere (Davis, 69°S), whereas earlier attempts at the Peruvian Antarctic station called 'Machu Picchu' (62°S) failed or showed much weaker PMSE compared to the NH (Balsley et al., 1993; Woodman et al., 1999; Morris et al., 2004). We speculate that the reason for these differences might be small SH/NH temperature differences increasing with decreasing latitude. Furthermore, some of these stations are located at similar geographical but very different geomagnetic latitudes. As mentioned above the interpretation of PMSE is more difficult compared to NLC since ionospheric and dynamic processes (turbulence) are involved.

Global circulation model (GCM) calculations of the solar cycle variations of the atmosphere at high latitudes during summer are now available. For example, Khosravi et al. (2002) predict a solar minimum/maximum decrease in temperature of 5 K and a water vapor increase of up to 70% at the polar summer mesopause region. According to our results presented in Fig. 7 and 9 one would expect an altitude variation of the peak NLC of 2.6 km due to temperature changes plus 1.6 km due to water vapor changes. These numbers are certainly larger compared to observations (Fiedler et al., 2003). We note that a recent long term analysis of HALOE temperatures shows a solar cycle modulation of approximately 5 K at 80 km (Hervig and Siskind, 2006). Assuming that the temperature variation is equally large (or even larger) at 85–90 km our model results and the observation of a nearly constant NLC altitude imply that the temperature effect on NLC must be compensated by other atmospheric changes, i.e. by vertical winds, etc.

In summary we have shown that ice layers at the summer mesopause region, detectable as NLC and PMSE, are sensitive indicators of atmospheric background changes. In this study we concentrate on temperature and water vapor changes. Non-linear processes such as freeze drying complicate the predictability of the impact of these changes on ice layer parameters. We have shown that the sensitivity (for example of maximum BSC altitude) can be even larger than expected from simple lapse rate considerations. This in turn implies that the observed steadiness of NLC heights observed over many years relates to very small temperature changes. A better understanding of ice particle related phenomena in the MLT region helps to understand long term and solar cycle induced changes of background conditions.

Acknowledgements

The project is funded by the Bundesministerium für Bildung, Wissenschaft, Forschung und Technologie, Bonn, under Grant 50 OE 99 01 (ROMA), and by the Deutsche Forschungsgemeinschaft under the CAWSES SPP Grant LU 1174/3-1 (SOLEIL).

References

Bailey, S.M., Merkel, A.W., Thomas, G.E., Carstens, J.N. Observations of polar mesospheric clouds by the Student Nitric Oxide Explorer. J. Geophys. Res. 110, doi:10.1029/2004JD005 422, 2005.

Balsley, B.B., Woodman, R.F., Sarango, M., Urbina, J., Rodriguez, R., Ragaini, E., Carey, J. Southern-hemisphere PMSE: where are they? Geophys. Res. Lett. 20, 1983–1985, 1993.

Berger, U., Lübken, F.-J. Weather in mesospheric ice layers. Geophys. Res. Lett. 33, doi:10.1029/2005GL024 841, 2006.

Berger, U., von Zahn, U. Icy particles in the summer mesopause region: three-dimensional modeling of their environment and two-dimensional modeling of their transport. J. Geophys. Res. 107, doi:10.1029/2001JA000 316, 2002.

Chu, X., Espy, P.J., Nott, G.J., Diettrich, J.C., Gardner, C.S. Polar mesospheric clouds observed by an iron Boltzmann lidar at Rothera (67.5°S, 68.0°W), Antarctica from 2002–2005: properties and implications. J. Geophys. Res., doi:10.1029/2006JD007086, 2006.

Fiedler, J., Baumgarten, G., von Cossart, G. Noctilucent clouds above ALOMAR between 1997 and 2001: Occurrence and properties. J. Geophys. Res. 108, 8453, 2003.

Gadsden, M., Schröder, W. Noctilucent clouds. Springer-Verlag, New York, 1989.

Hervig, M., Siskind, D. Decadal and inter-hemispheric variability in polar mesospheric clouds, water vapor, and temperature. J. Atmos. Solar Terr. Phys. 68, 30–41, 2006.

Hervig, M., Thompson, R., McHugh, M., Gordley III, L., Summers, M. First confirmation that water ice is the primary component of polar mesospheric clouds. Geophys. Res. Lett. 28, 971–974, 2001.

Höffner, J., Fricke-Begemann, C., Lübken, F.-J. First observations of noctilucent clouds by lidar at Svalbard, 78°N. Atmos. Chem. Phys. 3, 1101–1111, 2003.

Jensen, E., Thomas, G.E. Numerical simulations of the effects of gravity waves on noctilucent clouds. J. Geophys. Res. 99, 3421–3430, 1994.

Jensen, E., Thomas, G.E., Toon, O.B. On the diurnal variation of noctilucent clouds. J. Geophys. Res. 94, 14,693–14,702, 1989.

Khosravi, R., Brasseur, G., Smith, A., Rusch, D., Walters, S., Chabrillat, S., Kockarts, G. Response of the mesosphere to human-induced perturbations and solar variability calculated by a 2-d model. J. Geophys. Res., 107, doi:10.1029/2001JD001 235, 2002.

Körner, U., Sonnemann, G. Global 3d-modelling of the water vapor concentration of the mesosphere/mesopause region and implications with respect to the NLC region. J. Geophys. Res. 106, 9639–9651, 2001.

Lübken, F.-J. Seasonal variation of turbulent energy dissipation rates at high latitudes as determined by insitu measurements of neutral density fluctuations. J. Geophys. Res. 104, 13,441–13,456, 1997.

Lübken, F.-J. Thermal structure of the Arctic summer mesosphere. J. Geophys. Res. 104, 9135–9149, 1999.

Lübken, F.-J., Fricke, K.-H., Langer, M. Noctilucent clouds and the thermal structure near the Arctic mesopause. J. Geophys. Res. 101, 9489–9508, 1996.

Lübken, F.-J., Müllemann, A., Jarvis, M.J. Temperatures and horizontal winds in the Antarctic summer mesosphere. J. Geophys. Res. 107, doi:10.1029/2004JD005 133, 2004a.

Lübken, F.-J., Zecha, M., Höffner, J., Röttger, J. Temperatures, polar mesosphere summer echoes, and noctilucent clouds over Spitsbergen (78°N). J. Geophys. Res. 109, 2004b.

Morris, R.J., Murphy, D.J., Reid, I.M., Holdsworth, D.A., Vincent, R.A. First polar mesosphere summer echoes observed at Davis, Antarctica (68.6°S). Geophys. Res. Lett., 31, doi:10.1029/2004GL020 352, 2004.

Murphy, D.M., Koop, T. Review of the vapour pressure of ice and supercooled water for atmospheric applications, Quart. J.R. Met. Soc. 131, 1539–1565, 2005.

Nussbaumer, V., Fricke, K.-H., Langer, M., Singer, W., von Zahn, U. First simultaneous and common-volume observations of NLC and PMSE by lidar and radar. J. Geophys. Res. 101, 19,161–19,167, 1996.

Rapp, M., Lübken, F.-J. Polar mesosphere summer echoes (PMSE): review of observations and current understanding. Atmos. Chem. Phys. 4, 2601–2633, 2004.

Rapp, M., Thomas, G.E. Modeling the microphysics of mesospheric ice particles: assessment of current capabilities and basic sensitivities. J. Atmos. Solar Terr. Phys. 68, 715–744, 2006.

Rapp, M., Lübken, F.-J., Müllemann, A., Thomas, G., Jensen, E. Small scale temperature variations in the vicinity of NLC: experimental and model results. J. Geophys. Res. 107 (D19), 4392, doi:10.1029/2001JD001241, 2002.

Rapp, M., Lübken, F.-J., Hoffmann, P., Latteck, R., Baumgarten, G., Blix, T. PMSE dependence on aerosol charge number density and aerosol size. J. Geophys. Res. 108 (D8), 8441, doi:10.1029/2002JD002650, 2003.

Schmidt, H., Brasseur, G., Charron, M., Manzini, E., Giorgetta, M., Diehl, T., Fomichev, V., Kinnison, D., Marsh, D., Walters, S. The HAMMONIA chemistry climate model: sensitivity of the mesopause region to the 11-year cycle and CO_2 doubling. J. Climate 19, 3903–3931, 2006.

Siskind, D.E., Stevens, M.H., Englert, C.R. A model study of global variability in mesospheric cloudiness. J. Atmos. Solar Terr. Phys. 67, 501–513, 2005.

Toon, O.B., Turco, R.P., Hamill, P., Kiang, C.S., Whitten, R.C. A one dimensional model describing aerosol formation and evolution in the stratosphere; II. Sensitivity studies and comparison with observations. J. Atmos. Sci. 36, 718–736, 1979.

Turco, R.P., Hamill, P., Toon, O.B., Whitten, R.C., Kiang, C.S. A one dimensional model describing aerosol formation and evolution in the stratosphere; I. Physical processes and mathematical analogs. J. Atmos. Sci. 36, 699–717, 1979.

Turco, R.P., Toon, O.B., Whitten, R.C., Keesee, R.G., Hollenbach, D. Noctilucent clouds: simulation studies of their genesis, properties and global influences. Planet. Space Sci. 3, 1147–1181, 1982.

Woodman, R.F., Balsley, B.B., Aquino, F., Flores, L., Vazquez, E., Sarango, M., Huamann, M.M., Soldi, H. First observations of polar mesosphere summer echoes in Antarctica. J. Geophys. Res. 104, 22,577–22,590, 1999.